



High-Permittivity Polymer–Matrix Composites for the Development of Triboelectric Nanogenerators (TENGs) with Enhanced Performance: A Review

Adrián Urtecho¹ · Omar P. Troncoso¹ · Fernando G. Torres¹

Received: 18 April 2024 / Accepted: 24 May 2024 / Published online: 18 June 2024
© The Minerals, Metals & Materials Society 2024

Abstract

In recent years, the rapid increase in low-power electronics has shifted research focus towards new energy-harvesting devices. Triboelectric energy-harvesting technologies, such as triboelectric nanogenerators (TENGs), offer an efficient way to convert mechanical energy into electrical energy through the triboelectric effect. Polymers are used to fabricate crucial components in TENGs, acting as the triboelectric layers and storing electric charge. The dielectric properties of these polymers significantly influence the energy conversion capabilities of TENGs. High-permittivity polymer-based composites and nanocomposites have been studied for energy storage, such as capacitors, supercapacitors, and solar cells among others. These high-permittivity polymer composites can also be used to develop novel TENGs with high output performance. This paper reviews the development of high-dielectric-permittivity polymeric composites to be used as active triboelectric surfaces for TENGs with enhanced output performance. One strategy involves incorporating inorganic materials, semiconductors, conductors, and carbon-derived materials as an active phase within the polymer matrix. Other strategies, including the usage of polymeric fillers, coating, polarization, and ion implantation techniques, are also reported. This review may serve as a reference for optimizing polymer-based dielectrics in energy-harvesting-related areas. Through a deeper understanding of these techniques and materials, we can enhance the performance of TENGs to achieve high output efficiency.

Keywords Polymer dielectrics · triboelectric nanogenerators · permittivity · dielectric constant · ceramic fillers · percolative polymer composites

Introduction

In recent years, there has been a growing demand for powering new low-consumption electronic devices, driven by the emergence of the Internet of Things (IoT) and new mobile technologies. Sensors require a constant source of energy to ensure the transfer of information between these devices. In this context, new power generators/collectors have been developed to overcome the current limitations of power sources, such as batteries. These generators harness the mechanical energy of the environment to generate electrical energy using electrostatic, electromagnetic,

piezoelectric, and triboelectric effects.¹ Triboelectric nanogenerators (TENGs) take advantage of the triboelectric effect in conjunction with electrostatic induction.² These devices can generate electricity through friction or contact between two different materials, which are referred to as triboelectric surfaces. These active surfaces are crucial components of TENGs. Enhancing the capacity of these surfaces to store energy will improve the overall output of TENGs. This review explores the extensive research on polymer-based dielectrics with high permittivity. With the aim of enhancing the performance and energy conversion efficiency of TENGs, researchers have explored the unique electrical properties of high-permittivity polymers. The use of polymer composites and nanocomposites with high permittivity values provides a promising approach to enhance the efficiency of TENGs, enabling greater power generation and energy storage capabilities.

✉ Fernando G. Torres
fgtorres@pucp.pe

¹ Department of Mechanical Engineering, Pontificia Universidad Católica del Perú, Av. Universitaria, 1801 Lima, 32, Peru

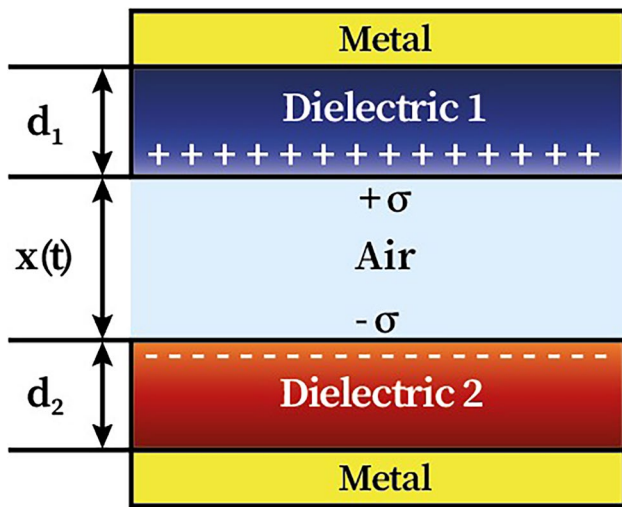


Fig. 1 Schematic representation of a contact-separation-mode TENG. Reprinted with permission from Niu et al.⁴

Working Principle of TENGs

TENGs generate electricity by utilizing the coupling effect of contact electrification and electrostatic induction. Figure 1 shows a contact-separation-mode TENG. In these TENGs, two different dielectric materials, with different electron affinities, are used as active surfaces. Two electrodes, typically composed of metals, are in contact with the dielectric layers. Before the active surfaces are in contact, there is no charge transfer and no potential difference between the two dielectric layers. When these layers are put into contact, due to the different electron affinities, one is negatively charged, while the other is positively charged. This phenomenon is known as contact electrification. Then the surfaces are separated, and the potential imbalance between them causes a flow of electrons in the external circuit until an equilibrium state is reached. A mechanical vibration allows the surfaces to be put in a contact-separation state, and thus an alternating current is generated. Contact electrification provides static polarized charges, and electrostatic induction is the main mechanism that converts mechanical energy into electricity.³

According to Niu et al.,³ the opposite static charges (tribo-charges) are uniformly distributed with equal density (σ) with negligible decay. The power generation of contact-separation TENGs can be modeled utilizing three parameters: the voltage (V) between the two electrodes, the amount of transferred charge (Q) in between, and the separation distance ($x(t)$) between the two triboelectric charged layers. The voltage between the two electrodes is given by the following equation^{5,6}:

$$V = -\frac{Q}{S\epsilon_0} \left(\frac{d_1}{\epsilon_{r1}} + \frac{d_2}{\epsilon_{r2}} + x(t) \right) + \frac{\sigma x(t)}{\epsilon_0} \quad (1)$$

where S , ϵ_0 , ϵ_{r1} , and ϵ_{r2} stand for the area of the active surfaces, the vacuum permittivity (dielectric constant), and the relative permittivity of dielectric layers 1 and 2, respectively. d_1 and d_2 represent the thickness of the dielectric layers (Fig. 1). According to Eq. 1, the output voltage increases with an increase in the relative permittivity of the dielectric layers.

Equation 1 describes the voltage generation of a case with an analytical solution. However, in any TENG, the electrical potential difference is derived from two contributions. The first part comes from the polarized triboelectric charges, which is a function of the separation distance, while the second part accounts for the already transferred charges Q . According to Niu et al.,³ the total voltage can be given by

$$V = -\frac{1}{C_{\text{TENG}}}Q + V_{\text{OC}} \quad (2)$$

The capacitance term (C_{TENG}) in Eq. 2 represents the inherent capacitance between the two electrodes. The V_{OC} term represents the open-circuit voltage originated from the separation of the polarized tribo-charges. Thus, any TENG can be idealized by the equivalent circuit shown in Fig. 2.

Figure 2 shows that TENGs have an inherent capacitive behavior. They can be considered as a voltage source coupled with a capacitance. It is worth noting that as in the case of any capacitor, the value of C_{TENG} is dependent on the voltage applied, size, and the relative permittivity (ϵ_r). The higher the

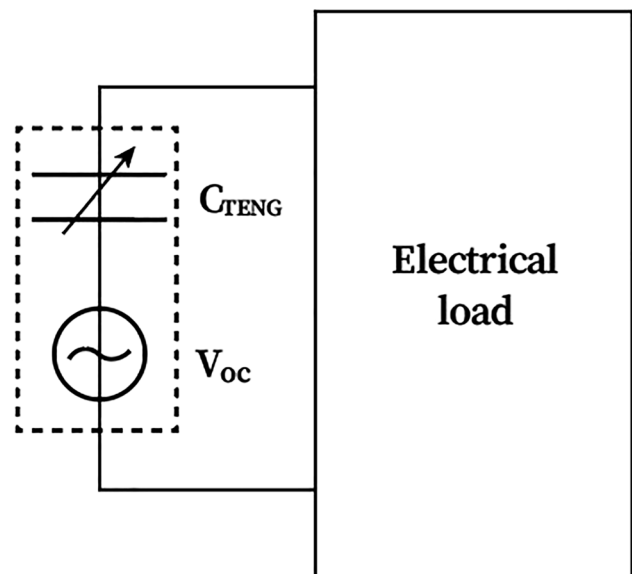


Fig. 2 Equivalent circuit of a TENG. Reprinted with permission from Niu and Wang.³

ϵ_r value, the larger the C_{TENG} value, and thus the better the electric performance.

Dielectric Properties of the Active Surfaces of TENGs

The previous discussion showed that the relative permittivity of the dielectric materials used as active surfaces should be as high as possible in order to maximize the power generation of TENGs. The relative permittivity is a measure of a material's ability to polarize in response to an applied field. Equation 3 shows the relationship between the capacitance (C) of a parallel plate capacitor and its size:

$$C = \epsilon_0 \epsilon_r \frac{A}{d} \quad (3)$$

where A and d stand for the area of the plates and separation distance, respectively. It is worth noting that in some contexts, relative permittivity is referred to as the dielectric constant (κ). For convenience, we will use the terms relative permittivity or simply permittivity throughout this review.

Equation 3 shows that permittivity (ϵ_r) accounts for the increase in capacitance when a dielectric is placed between the parallel plates of a capacitor. It is the ratio of the permittivity of this material to that of vacuum. The higher the relative permittivity of the dielectric, the higher the amount of energy it can store. A study of the polarization mechanisms in dielectrics will show that in the case of linear dielectrics (i.e., dielectrics whose permittivity is independent from the applied electric field, E), the energy storage density (U) can be calculated by Eq. 4⁷:

$$U = \epsilon_0 \epsilon_r E^2 \quad (4)$$

Thus, in the case of TENGs, the energy density is strongly dependent on the permittivity of the dielectrics used as triboelectric surfaces. Table I shows the relative permittivity of different materials. Most common polymers are linear dielectrics featuring a low permittivity. These linear dielectric polymers can be classified as polar or nonpolar. Examples of polar polymers include poly(methyl methacrylate) (PMMA), polyetherimide (PEI), polythiourea (PTU), and polysulfone (PSF), while examples of nonpolar polymers are polypropylene (PP) and polystyrene (PS).⁸ Ferroelectric polymers, which are polymers that exhibit permanent polarization due to polarized domains, are commonly utilized as nonlinear dielectric polymers.

Table I Relative permittivity of polymer dielectrics and other reference materials

Materials	Permittivity (ϵ_r)*
<i>Non-polymeric dielectric materials</i>	
TiO ₂	100
H ₂ O	78
Air	1.02
SiO ₂	3.9–4.5
Fluorosilicate glass	3.2–4.0
<i>Linear dielectric polymers</i>	
Neoprene	9.8
Polyimide (PI)	2.8–3.2
Fluorinated polyamide (FPA)	2.5–2.9
Methylsilsesquioxane	2.6–2.8
Polyarelene ether	2.8–2.9
Polyethylene (PE)	2.3–2.7
Polystyrene (PS)	2.5–2.9
Teflon AF (PTFE AF)	2.1
Poly(phenyl quinoxaline) (PPQ)	2.8
Poly(arylene ether) (PAE)	2.9
Polyquinoline	2.8
Silsesquioxane	2.8–3.0
Poly(norborene) (PNB)	2.4
Poly(ether ketone ketone) (PEKK)	3.5
Poly(arylene ether oxazole)	2.6–2.8
Polynaphthalene	2.2
Poly(tetrafluoroethylene) (PTFE)	1.9
Fluorinated poly(arylene ether)	2.7
Nonfluorinated aromatic polyimide	3.2–3.6
Polyetherimide (PEI)	3.3
Poly(methyl methacrylate) (PMMA)	3.49
Polycarbonate (PC)	2.8
Polyphenylene sulfide (PPS)	3
Polyethylene naphthalate (PEN)	3
Polyethylene terephthalate (PET)	3.3
Polyoxafluoronorborene (POFNB)	2.5
Polypropylene (PP)	2.25
Poly(2-(methylsulfonyl)ethyl methacrylate) (PMSEMA)	10.5
<i>Nonlinear dielectric polymers</i>	
Polyvinylidene fluoride (PVDF)	10
P(VDF-HFP)	8.6
P(VDF-TrFE)	8.5
P(VDF-CTFE)	13
P(VDF-TrFE-CFE)	50
P(VDF-TrFE-CTFE)	16

*Values were extracted from Refs. 7–9

Approaches Used to Enhance the Permittivity of Dielectric Polymers in TENGs

The control of the dielectric properties of the materials used as triboelectric surfaces in TENGs is a key factor in developing TENGs with high output performance. The permittivity of polymers depends on their ability to polarize in the presence of an electric field. There are five types of polarization mechanisms, including electronic, vibrational (or atomic), orientational (or dipolar), ionic (i.e., migration of ions), and interfacial polarizations.^{10–12} The development of strategies to enhance the permittivity of dielectric polymers must consider the types of polarizations that occur for a specific application. More than one type of mechanism may work simultaneously.

The most direct approach to developing TENGs with enhanced output performance is the use of polymer dielectrics with high permittivity. For instance, highly polarized polymers, such as polyvinylidene fluoride (PVDF) and its copolymers, feature high permittivity values (Table I). However, the permittivity of these ferroelectric polymers is still much lower than that of high-permittivity ceramics.¹³ One of the most common strategies for achieving high permittivity in dielectric polymers is to incorporate ceramics into a polymeric matrix. The ceramics used for the preparation of high-performance TENGs include titania (TiO₂), barium titanate (BaTiO₃), and strontium titanate (SrTiO₃), among others.

According to Popielarz et al.,¹⁴ in the case of a composite made from randomly dispersed ceramic particles (active phase) in a polymer matrix, the effective permittivity of the composite ($\epsilon_{r\text{-composite}}$) can be calculated using Eq. 5:

$$\log \epsilon_{r\text{-composite}} = \log \epsilon_{r\text{-matrix}} + \phi_{\text{filler}} \log \left(\frac{\epsilon_{r\text{-filler}}}{\epsilon_{r\text{-matrix}}} \right) \quad (5)$$

where ϕ_{filler} represents the volume fraction of the filler in the composite, while $\epsilon_{r\text{-filler}}$ and $\epsilon_{r\text{-matrix}}$ represent the permittivity of the filler and the polymer matrix, respectively.

The size of ceramic fillers significantly affects the dielectric properties of composites. Earlier research on polymer-based dielectric composites for the development of novel capacitors primarily focused on ceramic micro-fillers. However, the dielectric properties of these ceramic-polymer composites were compromised due to stress cracking and surface defects. Recently, there has been a preference for nanoscale ceramic fillers with a minimal volume fraction of the filler.^{15,16} Although ceramic-polymer nanocomposites feature high permittivity, they usually have poor mechanical properties, which limits their use in TENGs.

A different approach consists of using conductive or semiconductive fillers. These fillers significantly increase

ϵ_r due to the strong polarization at the conductor/insulator interfaces. The space charges (electrons and holes) accumulate at the filler-polymer interfaces, which triggers interfacial polarization.¹⁷ Metallic nanoparticles and conductive or semiconductive carbon nanostructures, such as carbon nanotubes and graphene, are commonly used as fillers.

Experimental results have shown that the conductivity of these conductive filler-polymer composites display a nonlinear increase in dielectric value when the concentration of fillers is above a percolation threshold. This behavior cannot be modeled by classical mixing rules but by percolation theories. Below this percolation threshold, the electrical properties of the composite are dominated by the matrix, as the conductive particles are isolated from each other. With increasing filler concentration, a connected network of conductive particles is formed through the component, resulting in a jump in the electrical conductivity.¹⁸ Experimental evidence shows that the permittivity of these composites increases to the vicinity of the percolation threshold (f_c) and can be described by the following power law^{19–22}:

$$\frac{\epsilon_{r-c}}{\epsilon_{r-m}} \propto |f_c - f|^{-S} \quad (6)$$

where ϵ_{r-m} represents the permittivity of the polymer matrix, f denotes the volume fraction of the filler, and S is an exponent approximately equal to 1.

The volume fraction of the conductive filler must be slightly below the percolation threshold. If the percolation threshold is reached, the fillers would form a conduction pathway along the percolated polymer, and the composite would become a conductive material, preventing the TENG from functioning. In order to achieve a high permittivity and prevent particle percolation, the nanoparticle content must be precisely controlled.

TENGs Based on Dielectric Polymers and Inorganic fillers

Among the strategies to enhance the permittivity of polymers used as triboelectric layers, one approach is to incorporate a second phase with higher permittivity into the matrix. This helps to improve the overall permittivity of the polymeric composite. Table II shows a summary of the TENGs fabricated using dielectric polymers reinforced with inorganic ceramics studied in this section.

The addition of ceramic nanoparticles is used to enhance the properties of the triboelectric layers. For example, Chen et al.²⁴ studied the increase in relative permittivity achieved by incorporating high-dielectric nanoparticles and reducing

Table II Electrical output of TENGs based on polymer/inorganic filler dielectrics

Matrix	Inorganic fillers	Filler content (%)	Electrical output		Refs.
			Without fillers	With fillers	
PVDF-TrFE/aluminum	BaTiO ₃ (BTO) NPs			1130 V; 1.5 mA	23
Porous PDMS (15%vol pores)	SrTiO ₃ NPs	10 v%		338 V; 9.06 $\mu\text{A}/\text{cm}^2$	24
	–		257 V; 6.6 $\mu\text{A}/\text{cm}^2$		24
Pure PDMS (0%vol of pores)	SrTiO ₃ NPs	10 v%	172 V; 2.98 $\mu\text{A}/\text{cm}^2$	305 V; 7.18 $\mu\text{A}/\text{cm}^2$	24
	SiO ₂ NPs	1–25 v%		170 V; 2.9 $\mu\text{A}/\text{cm}^2$	24
	TiO ₂ NPs	8 v%		235 V; 6 $\mu\text{A}/\text{cm}^2$	24
	BaTiO ₃ (BTO) NPs	10 v%		260 V; 6.5 $\mu\text{A}/\text{cm}^2$	24
PVDF	BaTiO ₃ (BTO) NPs	40 w%	196 V; 8.84 mA	412 V; 183.4 mA	25
	BaTiO ₃ (BTO) NPs	80 w%		810 V; 36.2 mA	25
Bacterial cellulose (BC) nanofiber film	BaTiO ₃ (BTO) NPs	13.5 w%	120 V; 9.7 μA	181 V; 21 μA	26
Porous PDMS	BaTiO ₃ (BTO) NPs	7 w%		2500 V; 150 μA	27
PVDF	BTO@PtBA	30 w%	2.4 $\mu\text{A}/\text{cm}^2$	6.1 $\mu\text{A}/\text{cm}^2$	28
	BTO@HBP@PMMA	30 w%			29
PVDF-TrFE/Nylon 11	Zirconium oxide (ZrO ₂) NPs-PMMA	–0.5–25 w%	100 V; 100 μA	150 V; 300 μA	30
PVB	PZT	0.15 v%			31
PDMS	BZTO	20 w%		376	32
Nylon 11	MoS ₂	0.5 w%	400 mV	733 mV	33
PVDF-TrFE	MoS ₂	0.5 w%	–300 mV	–726 mV	33
Natural rubber (NR)	TiO ₂ NPs	0.5 w%	60 V; 5 μA	204 V; 13 μA	34
PDMS	Calcium copper titanate (CCTO) nanocrystals	30 w%	30 V; 10 mA/m ²	210 V; 170 mA/m ²	35

the thickness through the creation of pores in PDMS films, as shown in Fig. 3. Among the nanoparticles studied were SiO₂ ($\epsilon_r = 3$, the same as that of PDMS), TiO₂ ($\epsilon_r = 80$), BaTiO₃ ($\epsilon_r = 150$), and SrTiO₃ ($\epsilon_r = 300$) NPs. The best performance of TENGs was achieved by increasing the filling volume of NPs and pores until reaching a maximum point. After that point, the performance began to decrease. It was explained that the reduction of the effective friction area of PDMS was due to the presence of nanoparticles on the surface. The best electrical output was achieved by incorporating 10 vol% of SrTiO₃ nanoparticles and 15 vol% of pores in the PDMS. This TENG exhibited an open-circuit voltage of 338 V and a short-circuit current density of 9.06 $\mu\text{A}/\text{cm}^2$ at a frequency of 2.5 Hz. These values were higher than the 305 V and 7.18 $\mu\text{A}/\text{m}^2$ for flat PDMS with 10 vol% SrTiO₃ NPs, 257 V and 6.6 $\mu\text{A}/\text{m}^2$ for the sponge PDMS-based TENG with 15 vol% pores without NPs, 170 V and 2.9 $\mu\text{A}/\text{m}^2$ for flat PDMS with 1–25 vol% SiO₂ NPs, 235 V and 6 $\mu\text{A}/\text{m}^2$ for flat PDMS with 8 vol% TiO₂ NPs, 260 V and 6.5 $\mu\text{A}/\text{m}^2$ for flat PDMS with 10 vol% BaTiO₃ NPs, and 172 V and 2.98 $\mu\text{A}/\text{cm}^2$ for flat pure PDMS TENG.

One of the most commonly used enhancing materials is barium titanate (BaTiO₃), a ceramic with high permittivity ($\epsilon_r = 150$). For example, Seung et al.²³ studied the

effect of incorporating barium titanate (BTO) nanoparticles into a polarized ferroelectric copolymer matrix, poly(vinylidene fluoride-co-trifluoroethylene) [P(VDF-TrFE)]. They found that polarization and the incorporation of BTO nanoparticles have a synergistic effect on improving the electrical performance of a TENG with aluminum as the triboelectric positive layer. This TENG exhibited an open-circuit voltage of 1130 V and a short-circuit current of 1.5 mA when a force of 6 kgf was applied at a frequency of 5 Hz.

Another design of a TENG based on a nanocomposite film of poly(vinylidene fluoride) (PVDF) and barium titanate (BaTiO₃) nanoparticles demonstrated that the inclusion of BaTiO₃ nanoparticles enhanced the output performance of the TENG.²⁵ The performance continued to improve until it reached a peak at the addition of 40 wt% BaTiO₃ nanoparticles. The open-circuit voltage (V_{oc}), short-circuit current (I_{sc}), and transferred charge (Q_{sc}) were 412 V, 183.4 mA/m², and 57.3 $\mu\text{C}/\text{m}^2$, respectively. It was higher than the pure PVDF TENG (196 V, 8.84 mA/m², and 30.3 $\mu\text{C}/\text{m}^2$). Zheng et al.²⁵ proposed developing a thin layer above the PVDF@BTO composite film to take advantage of the high permittivity of concentrations above 40 wt% BTO. The PVDF@BTO exhibited different permittivity

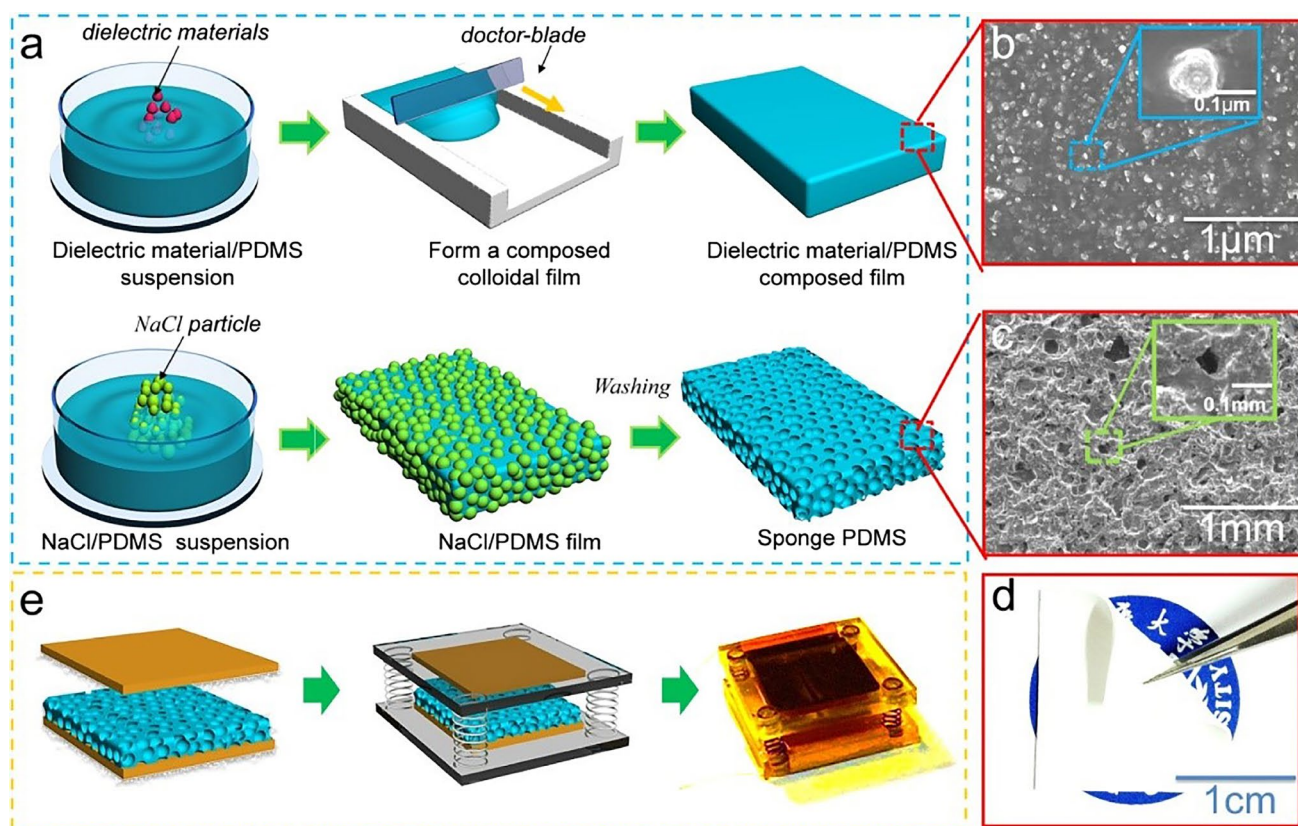


Fig. 3 Processing routes for the preparation of PDMS-based active layers and a TENG fabricated using them. (a) Schematic diagram of the fabrication process for a dielectric material/PDMS composite film and a NaCl/PDMS sponge. Scanning electron microscopy (SEM) image of the cross section of the (b) dielectric material/PDMS com-

posite film and the (c) NaCl/PDMS sponge. (d) Digital photograph of the composite sponge film. (e) Schematic diagram of the fabrication process of the PDMS-based TENG. Reprinted with permission from Chen et al.²⁴

values at various concentrations. PVDF@80BTO had a higher permittivity of 140 at 100 Hz compared to 70 for PVDF@60BTO and 30 for PVDF@60BTO at the same frequency. Finally, they used the nanocomposite film with PVDF that was spin-coated at 3000 rpm. After coating the PVDF@80BTO, the permittivity was reduced from 140 to 100 at 100 Hz. However, the output performance was the highest compared to the others. This TENG exhibited a V_{oc} of 810 V, J_{sc} of 36.2 mA/m², and Q_{sc} of 100.4 μ /Cm².

Tantraviwat et al.²⁷ improved the output performance of a porous PDMS-based TENG by incorporating BaTiO₃ (BTO) particles into the matrix. The best TENG performance was achieved with 7 wt% BTO particles and at a frequency of 5 Hz. This resulted in a V_{oc} (open-circuit voltage) of 2500 V, I_{sc} (short-circuit current) of 150 μ A, and a maximum power density of 1.2 W/m². Beyond this concentration, the surface charge density and the electrical output of the TENG performance began to drop. The permittivity continued to increase, but agglomeration of the particles started to be observed. Additionally, the porosity and rugosity started to decrease, which explains the loss of performance.

BaTiO₃ (BTO) particles can also be incorporated into a bacterial cellulose (BC) nanofiber film to simultaneously improve the dielectric properties and surface roughness.²⁶ BaTiO₃ particles were introduced into a BC film through vacuum filtration to obtain a BC/BaTiO₃ composite film. The best electrical output performance of the fabricated TENGs was achieved by introducing 13.5% BaTiO₃. It exhibited an open-circuit voltage of 181 V and a short-circuit current of 21 μ A when a peak force of 42 N was applied at a frequency of 2 Hz. These values were higher than the 120 V and 9.7 μ A for the pure BC TENG, 130 V and 14.8 μ A for the BC/5% BaTiO₃ composite TENG, and 150 V and 19 μ A for the BC/25% BaTiO₃ composite TENG. The decrease in electrical output for a TENG with a BaTiO₃ composite containing more than 13.5% nanoparticles (NPs) can be attributed to the increase in surface roughness caused by NP aggregation.

Other researchers have investigated the utilization of BTO as the core material in a core-shell nanoparticle composite. Xie et al.²⁹ created a spherical polymer nanocomposite consisting of a BTO core and two shells: hyperbranched

aromatic polyamide (HBP) and poly(methyl methacrylate) (PMMA). The first shell, HBP, was grafted onto the surface of the BaTiO₃ nanoparticles. The second shell, PMMA, was grafted onto the terminal groups of HBP using atom transfer radical polymerization (ATRP). The nanocomposite BTO@HBP@PMMA exhibited higher permittivity and lower dielectric loss compared to BTO nanoparticles and BTO@HBP nanocomposites. The reason is that the nanocomposite leverages the properties of both the layers and the core, resulting in a synergistic effect. The BTO nanoparticles and HBP layer have high permittivity and high electrical conductivity, but they also exhibit a high dielectric loss. PMMA, on the other hand, has a relatively low permittivity and low dielectric loss. The permittivity of the nanocomposite BTO@HBP@PMMA increases with the concentration of BTO nanoparticle loading. The best performance was achieved with a BTO content of approximately 56.7 vol%, resulting in a permittivity of 39.3 at 1 kHz. In comparison, the permittivity for PMMA was 3.7, while for the BTO/PMMA nanocomposite, it was 33, both measured at the same frequency. The dielectric loss content was even lower at 0.028 at 1 kHz compared to a dielectric loss of 0.042 for PMMA and 0.039 for BTO/PMMA nanocomposite at the same frequency. These results demonstrate the significant potential of the nanocomposite BTO@HBP@PMMA for use in developing triboelectric layers for TENGs.

In another study, Du et al.²⁸ investigated the effect of incorporating core–shell nanoparticles into a PVDF matrix. These nanoparticles were based on BaTiO₃ nanoparticles (BTO NPs) and were capped with poly(tert-butyl acrylate) (PtBA). The nanoparticles were synthesized using ATRP. The study also examined the effect of the ion injection method. The PtBA reduced the surface energy, helped prevent the aggregation of BTO NPs, and provided a net dipole moment to the film through its ester groups. The permittivity of pure PVDF increased from 8.5 to 15 with the incorporation of 30 wt% of BTO@PtBA NPs. The TENG based on this composite film exhibited a higher current density of 2.1 $\mu\text{A}/\text{cm}^2$ compared to the 0.8 $\mu\text{A}/\text{cm}^2$ obtained by the TENG using a pure PVDF film. The best performance of the TENG was achieved after applying an ion injection method to a nanocomposite film of barium titanate (BTO)@poly(tert-butyl acrylate) (PtBA) (30% w/w) and polyvinylidene fluoride (PVDF). This TENG exhibited a higher current density of 6.1 $\mu\text{A}/\text{cm}^2$ compared to the other TENGs. In contrast, the TENG based on pure PVDF film achieved a current density of 2.4 $\mu\text{A}/\text{cm}^2$ after the ion injection method was applied.

Zirconium derivatives, such as zirconium oxide (ZrO₂), also display interesting properties. With the insertion of zirconium oxide (ZrO₂) NPs³⁰ into ferroelectric layers of PVDF-poly(trifluoroethylene) (TrFE) and PMMA into

Nylon 11 films, the PVDF-TrFE/ZrO₂ NPs and Nylon 11/PMMA composite layers acted as the triboelectric positive and negative layers, respectively. The current density was measured independently for both composite layers. The maximum current densities were achieved by incorporating 0.5 wt% of ZrO₂ NPs and 25 wt% of PMMA into their respective layers. The obtained values for the current density were 200 $\mu\text{A}/\text{cm}^2$ for the PVDF-TrFE/ZrO₂ NPs layer and 160 $\mu\text{A}/\text{cm}^2$ for the Nylon 11/PMMA layer. These values were higher than those of their non-modified counterparts, which were 110 $\mu\text{A}/\text{cm}^2$ for the PVDF-TrFE film and 110 $\mu\text{A}/\text{cm}^2$ for the Nylon 11 film. Beyond these concentrations, the current density started to decrease drastically. This decrease was explained by observing exposed NPs on the surface. The TENG made with these composite layers exhibited an improvement compared to the non-modified layers. The open-circuit voltage and short-circuit current increased from 100 V and 100 $\mu\text{A}/\text{cm}^2$ to 150 V and 300 $\mu\text{A}/\text{cm}^2$, respectively. Cao et al.³⁰ also investigated the effect of polarization on these ferroelectric composite layers. The surface potential of poled composite layers, measured by an electrostatic voltmeter, showed that the best configuration was achieved with the forward polarization of Nylon 11/PMMA and the reverse polarization of PVDF-TrFE/ZrO₂ composite layers. These values, measured at 75 V for Nylon/PMMA and -70 V for PVDF-TrFE/ZrO₂, were higher than the values of the unpoled layers, which were 25 V and -28 V, respectively. The TENG fabricated with these poled composite layers demonstrated the best performance, achieving an open-circuit voltage of 500 V and a short-circuit current density of 500 $\mu\text{A}/\text{cm}^2$, resulting in a maximum power density of 42 mW/cm^2 .

Another derivative of zirconium is zirconate titanate (PZT), which is a ferroelectric crystal–ceramic. This material was added to a polyvinyl butyral (PVB) matrix to enhance the permittivity.³¹ The highest permittivity of 155 and a low dielectric loss of 0.05 at a frequency of 100 Hz were achieved with a PVB volume fraction of 0.15. This composite layer shows good potential for use in electrical energy storage devices and electrical nanogenerators, such as TENGs.

Wang et al.³² designed a hybrid generator (HG) PENG/TENG with two PDMS-based composite films. The electrical output performance of the PENG and TENG was improved by the incorporation of (Ba_{0.838}Ca_{0.162})(Ti_{0.9072}Zr_{0.092})O₃ (BCZTO) and Ba(Ti_{0.8}Zr_{0.2})O₃ (BZTO) into PDMS, respectively. The permittivity increased from 3 for pure PDMS to ~ 6 for BCZTO 40 wt%/PDMS and 10 for BZTO 20 wt%/PDMS. The electrical output of the unpoled PDMS/BZTO-based TENG was ~ 60 V with 20 wt% BZTO higher than pure PDMS TENG (~ 28 V) under a vertical force of 20 N. After polarizing this layer, the poled PDMS/BZTO-based TENG reached an open-circuit voltage of ~ 132 V. The

HG consisted of a three-electrode configuration connected to a rectifier circuit. The poled PDMS/BZTO TENG in this configuration exhibited an open-circuit voltage of 376 V, with a maximum instantaneous power density of 3.5 W/m². The whole HG exhibited an open-circuit voltage of 390 V and a current density of 47 mA/m² after rectification.

Kim et al.³³ doped both Nylon 11 and PVDF-TrFE films with MoS₂ flakes to enhance the output performance of a TENG based on these composite films. The ferroelectric Nylon 11/MoS₂ and PVDF-TrFE/MoS₂ composites worked as positive and negative triboelectric layers. The TENG output performance increased with MoS₂ content until it reached the concentration 0.5 wt%. Then a high-voltage poling process was performed to maximize the surface charge density of composite films. The surface potential increased from 400 mV for unpoled Nylon 11 film to 733 mV for Nylon 11/MoS₂ film, and from -300 mV for PVDF-TrFE film to -726 mV for PVDF-TrFE/MoS₂ film. The TENG based on these poled composite films exhibited a peak-to-peak output voltage of 270 V, peak-to-peak current density of 645 $\mu\text{A}/\text{cm}^2$, and an output power density of 50 mW/cm². These values were higher than $V_{\text{pp}} = 150$ V and $J_{\text{pp}} = 130$ $\mu\text{A}/\text{cm}^2$ obtained in the non-modified Nylon 11:PVDF-TrFE TENG and $V_{\text{pp}} = 240$ V and $J_{\text{pp}} = 323$ $\mu\text{A}/\text{cm}^2$ obtained in the unpoled Nylon 11/MoS₂:PVDF-TrFE/MoS₂ TENG.

There are also other titanium derivative materials that can enhance the dielectric properties of polymers: titanium oxide (TiO₂) and CCTO (CaCu₃Ti₄O₁₂). The insertion of TiO₂ nanoparticles into a polymer, natural rubber (NR) film, to develop a TENG device was evaluated by Bunriw et al.³⁴ The insertion of TiO₂ NPs (0.1 to 0.5 wt%) into the NR film did not produce a significant improvement of electrical output. This low improvement was explained by the rapid agglomeration and poor dispersion in the NR matrix. The ball-milling process was adopted to produce a better distribution in NR matrix. After 24 h of ball milling, the NR-TiO₂ NP-based TENG showed a better distribution in the matrix. The best electrical output of the TENG was achieved by the introduction of 0.5 wt% of TiO₂ NPs and after 24 h of ball milling. This TENG exhibited an open-circuit voltage of 204 V and a current of 13 μA when a force of 10 N was applied at a frequency of 10 Hz. These values were higher than those obtained by the pure NR-based TENG (60 V and 5 μA at a 5-Hz frequency) and the other TENGs with shorter milling time, lower concentration of NPs, and lower frequencies.

Fang et al.³⁵ incorporated CaCu₃Ti₄O₁₂ (CCTO) nanocrystals into a PDMS matrix to increase the permittivity. The PDMS surface was modified using simple template transfer method based on a textured fluorine-doped tin oxide (FTO)-coated glass to obtain a micro/nano texture. BaTiO₃ (BTO) nanoparticles were also studied to

be compared. Transmission electron microscopy (TEM) images showed the distance of lattice strips in BTO was 1.8 Å, corresponding to the (210) plane of the tetragonal phase BTO. The lattice planes of CCTO were visible, with a d spacing of 2.61 Å, corresponding to the (220) plane.

Some TENGs in contact-separation mode were fabricated with different concentrations of CCTO and BTO, which acted as the negative triboelectric layer, while a P(VDF-TrFE) film served as the positive triboelectric layer. The best performance was achieved with the incorporation of 30 wt% of CCTO, resulting in an open-circuit voltage of 210 V, a current density of 170 mA/m², and a charge density of 108 $\mu\text{C}/\text{m}^2$. The TENG with 30 wt% BTO exhibited a V_{oc} of 150 V, and a charge density of 108 $\mu\text{C}/\text{m}^2$. Both values were higher than those of TENGs based on FTO PDMS (V_{oc} of 80 V and a charge density of 55 $\mu\text{C}/\text{m}^2$) and flat PDMS (V_{oc} of 30 V and a charge density of 26 $\mu\text{C}/\text{m}^2$).

CCTO-Ni composites were also fabricated by Chi et al. by depositing Ni nanoparticles onto the CCTO via electroless plating.³⁶ These fillers were introduced into the PVDF matrix through melt mixing. The CCTO@Ni/PVDF composite film, containing 5% volume of fillers and subjected to a 30-min magnetic field treatment (1 T) at 160°C, exhibited the best dielectric properties. The dielectric permittivity of this film was 1.41×10^4 at 10 Hz, higher than that of PVDF with a value of 10. The CCTO@Ni/PVDF composite film without magnetic treatment had a permittivity of 12. The other films, which underwent 1 h and 2 h of magnetic treatment, also had a permittivity of around 12 at the same frequency. The conductivity and dielectric loss tangent reached their maximum after 30 min of magnetic treatment. These higher values in permittivity, conductivity, and loss tangent can be explained by the percolation effect, which causes an insulating/conducting phase transition and conductive loss. The CCTO@Ni/PVDF film with magnetic treatment shows interesting potential for use in energy storage applications. However, the dielectric loss and conductivity need to be addressed.

TENGs Based on Dielectric Polymers and Conductive Fillers

As discussed in Section "Approaches Used to Enhance the Permittivity of Dielectric Polymers in TENGs," another strategy to improve the permittivity of the triboelectric layers is the addition of a conductive material that has a higher permittivity as a second phase in the matrix, thus improving the overall permittivity of the composite. But studies have found that the improvement is bounded to the percolation theory, which shows that the addition of a conductive material does not make the composite conductive until it reaches the percolation threshold, where it drastically changes its

Table III Electrical output of TENGs based on polymers/conductive filler dielectrics

Matrix	Inorganic fillers	Filler content	Electrical output		Refs.
			Without fillers	With fillers	
PDMS	Silver (Ag) NPs	20	–	33.6 V; 5.1 μ A	37
	Copper (Cu) NPs	–	–	30.64 V; 3.83 μ A	37
	Aluminum (Al) NPs	–	–	32.17 V; 4.24 μ A	37
	Zinc (Zn) NPs	–	–	25.52 V; 3.27 μ A	37
	Tin (Sn) NPs	–	–	24.49 V; 3.03 μ A	37, 38
PDMS@PDA	Gold (Au) NPs	–	33 V	107 V; 2 μ A	38
PDMS	Gold (Au) NPs	0.28	5 V; 0.006 μ A	50 V; 0.62 μ A	39
Natural rubber (NR)	Silver (Ag) NPs	–	50 V; 4.3 μ A	120 V; 10.7 μ A	40
Chitosan (CS)	Silver (Ag) nanowires (NWs)	0.20 wt%	17.1 V; 0.9 μ A	36.4 V; 2.3 μ A	41
Kapton	Silver (Ag) NWs	–	–	3600 V; 9 μ A	42
Cellulose aerogel paper/PDMS.	BaTiO ₃ (BTO) NPs/Silver (Ag) NPs	3–1 w%	30 V; 3 μ A	88 V; 8.3 μ A	43
PVDF	BaTiO ₃ (BTO) NPs/Silver (Ag) NPs	35 v%	–	10 ⁻¹² S cm ⁻¹	44
Bacterial cellulose (BC)	BaTiO ₃ (BTO) NPs/Silver (Ag) NWs	–	44 V; 1.6 μ A	170 V; 9.8 μ A	45
PVDF	CCTO@NI	5 v%	$\epsilon_r = 12$	$\epsilon_r = 1.41 \times 10^4$	36
Cellulose aerogel	CNTs	1 w%	–	100 V; 8 μ A	46
Cement@HEC	CB NPs	0.25 w%	39 V; 3.3 μ A	109 V; 9.1 μ A	47
PDMS	GPs	3 w%	16.5 μ A; 3.7 W/m ²	4.5 μ A; 1.4 W/m ²	48
PDMS	GO	4 mg/mL	125 V; 14 μ A	218 V; 25 μ A	49
Sodium dodecyl sulfate (SDS)	GO	0.2 M	125 V; 14 μ A	331 V; 33 μ A	49
PVA-PAAm/GPPD hydrogel	GO NSs	–	–	210 V	50

behavior. Near this threshold is where we have the maximum improvement. Table III shows a summary of the TENGs and materials reviewed in this section.

Metallic Fillers

Anlin et al.³⁷ studied the incorporation of various metal nanoparticles into a polydimethylsiloxane (PDMS) matrix at different weight percentages. The permittivity of metal/PDMS composite films and the electrical output performance of metal/PDMS composite-based TENGs showed an increasing tendency as the filler weight percent increased up to 20 wt%. Beyond this concentration, the agglomeration of nanoparticles had a negative effect on all properties. The best TENG performance was achieved with 20 wt% of silver (Ag) NPs at a frequency of 10 Hz and applied force of 10 N. This Ag/PDMS composite-based TENG exhibited an open-circuit voltage of 33.6 V and short-circuit current of 5.1 μ A. These values were higher than those of the PDMS composite film based on copper, which had a voltage of 30.64 V and a current of 3.83 μ A. Similarly, the values were higher than those of the aluminum film (32.17 V and 4.24 μ A), zinc film (25.52 V and 3.27 μ A), and tin film (24.49 V and 3.03 μ A) under the same conditions.

Another metal used to enhance dielectric properties is gold. Gold nanoparticles can be inserted into porous polydimethylsiloxane (PDMS) by introducing polydopamine

(PDA) as a dispersant agent.³⁸ These Au nanoparticles (Au NPs) exhibited a negative surface charge (zeta potential = -33.2 mV), which hinders their adsorption onto the hydrophobic surface of the PDMS sponge. PDA reduces the hydrophobicity of PDMS and enhances the chemical binding to Au NPs through the introduction of catechol groups. After the in situ polymerization of dopamine monomers in the PDMS sponge, Au NPs were uniformly introduced into the PDMS matrix. The concentration of Au NPs was controlled by the immersion time of PDA-coated particles. The permittivity monotonically increased from 2.94 for PDMS to 3.70 for PDMS/PDA/Au NPs with increasing immersion time, while the dielectric loss remained nearly unaltered. The best output performance of the PDMS/PDA/Au-based TENG was achieved with an immersion time of 24 h. This TENG exhibited an open-circuit voltage of 107 V and a short-circuit current of 2 μ A (Fig. 4). This voltage was higher compared to the 33 V voltage shown by the non-modified PDMS TENG and the 65 V shown by the PDMS/Au TENG.

Another study of the same combination, Au/PDMS, was conducted by Chun et al.³⁹ They assessed the impact of pores in mesoporous PDMS film and the concentration of Au NPs embedded in the PDMS film on the electrical output performance of vertical contact–separation-mode TENGs. Mesoporous PDMS was fabricated by casting a mixture of PDMS solution and deionized (DI) water containing Au NPs. After the evaporation of water, Au NPs were found

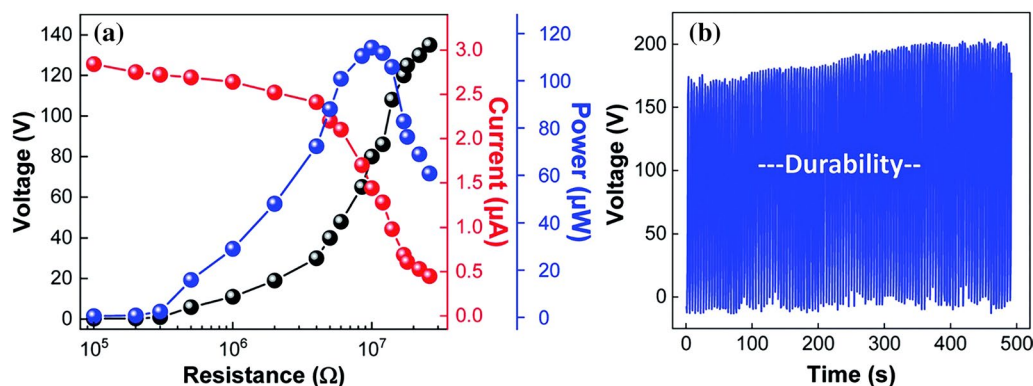


Fig. 4 (a) Output voltage (black), current (red), and power (blue) of a PDMS/PDA/Au-based TENG. (b) Stability and durability test of such a TENG under a periodic contact–separation processes. Reprinted with permission from Biutty et al.³⁸ (Color figure online)

exclusively within the pore walls. This behavior can be explained by the high hydrophobicity of PDMS, which tends to form spherical shapes. This distribution of Au NPs resulted in aligned dipoles due to the charges generated upon the contact with PDMS. The electrical output performance was improved by increasing the concentration of Au NPs and the density of pores. The best electrical output was achieved with a porosity of 59% and the addition of 0.28 wt% Au nanoparticles. This TENG exhibited a V_{oc} of 50 V and a J_{sc} of 0.62 $\mu\text{A}/\text{cm}^2$ under a compressive force of 90 N at a frequency of 5 Hz. These values were higher than the 5 V and 0.006 $\mu\text{A}/\text{cm}^2$ obtained in the non-modified PDMS-based TENG. It also showed that with higher porosity, the contact surface area increases. Additionally, a higher concentration of Au NPs leads to a higher permittivity. Both effects combined resulted in an enhancement of the electrical output of the TENG.

Silver nanoparticles (Ag NPs) are widely used in nanocomposites. Appamato et al.⁴⁰ conducted a study on the effect of inserting these nanoparticles, which were capped by two capping agents, into a natural rubber polymer matrix. The different capping agents used were anionic [sodium dodecyl sulfate (SDS)] and cationic [cetyltrimethylammonium bromide (CTAB)] surfactants. The best permittivity and TENG performance were achieved by using CTAB (5 mM). The improved performance was attributed to the smaller particle size achieved and the interparticle distance of CTAB-capped Ag NPs. It was noted that the interaction between CTAB and the NR molecules enhanced the electron-donating ability of the NR composite film. This NR-Ag composite film exhibited a permittivity of 8.12 at 1 kHz, compared to the non-modified NR film (6.50), NR@SDS, and NR@CTAB films with different concentrations (ranging from 6.72 to 7.72). The TENG output performance was a V_{oc} of 120 V and an I_{sc} of 10.7 μA in comparison to the non-modified NR-based TENG with values of 50 V and 4.3 μA . The other TENGs with SDS and

CTAB concentrations had values ranging from 54 to 90 V for V_{oc} and from 4.8 to 8.1 μA for I_{sc} .

Other forms of Ag-based nanocomposites include the addition of nanowires (Ag NWs). Zhang et al.⁴¹ inserted these nanowires into a chitosan (CS)-based film to enhance its dielectric properties. This composite film, consisting of CS/Ag NWs, was utilized in the production of a TENG operating in vertical contact-separation mode. It was composed of a PVDF film as a tribo-negative layer and the CS/Ag NWs composite film as a tribo-positive layer. The highest performing TENG was achieved by incorporating 0.20 wt% of Ag NWs at a frequency of 3 Hz. This TENG exhibited an I_{sc} of 2.3 μA , V_{oc} of 36.4 V, and a transfer charge quantity of 12.3 nC, which is higher than the values obtained in the non-modified pure CS-based TENG. The non-modified TENG had an I_{sc} of 0.9 μA , V_{oc} of 17.1 V, and 7.2 nC. This increase was explained by the formation of nanocapacitors between conductive silver nanowires (Ag NWs). Higher concentrations above 0.20% resulted in decreased output performance, likely due to the exposure of Ag NWs on the surface. Oh et al.⁴⁵ incorporated silver nanowires (Ag NWs) and BaTiO₃ nanoparticles (BTO NPs) into a bacterial cellulose (BC) matrix to produce a ferroelectric cellulose composite film. This film was used as a positive triboelectric layer and electrode simultaneously in the development of a TENG. After undergoing a high-voltage poling process, the TENG based on the poled BC/Ag NW/BTO NP composite achieved the best performance. It generated a maximum voltage of 170 V, a maximum current of 9.8 μA , and a maximum power density of 180 $\mu\text{W}/\text{cm}^2$ when a force of 5 kgf was applied. This electrical output was higher than the unpoled BC/Ag NW/BTO NP (~55 V and ~3 μA), BC/Ag NW (~60 V and ~2.8 μA), and the non-modified BC-based TENG (44 V and 1.6 μA).

Another single-electrode TENG was fabricated using a Kapton film with a nano-patterned structure of Ag nanowires.⁴² It was designed to modify the transmittance

of a smart optical modulator (SOM) from 72% to 40%. The distribution of nanowire arrays on the surface was created using inductively coupled plasma (ICP) reactive ion etching. The nanowires have an average diameter of about 300 nm. This Kapton-based TENG exhibited an open-circuit voltage of 3600 V and a short-circuit current of 9 μ A.

Conductive fillers can also be added with nonconductive fillers to obtain a three-phase system. For instance, Shi et al.⁴³ inserted BaTiO₃ (BTO) and Ag NPs into a cellulose aerogel paper and a polydimethylsiloxane (PDMS) matrix. These materials are typically used as positive and negative triboelectric layers in the fabrication of TENGs, respectively. The incorporation of BTO and Ag NPs into these materials increased the output performance of the TENG from 30 V and 3 μ A to 88 V and 8.3 μ A with an applied force of 12 N at a frequency of 3 Hz. The maximum values were achieved when the concentration of BTO and Ag nanoparticles in cellulose and PDMS was 3 and 1 wt%, respectively. The dielectric spectroscopy revealed the effect of the incorporation of these nanoparticles. The 5 wt% BTO nanoparticles added to cellulose increased the permittivity from 3.06 of pure cellulose to 6.25 at 1 kHz. The 1 wt% Ag

NPs in PDMS increased the permittivity from 2.45 to 2.95 at 1 kHz.

Ren et al.⁴⁴ achieved higher permittivity in PVDF by incorporating Ag/BaTiO₃ nanocomposites instead of using only pure BTO NPs as fillers. The BTO@Ag hybrid nanoparticles were prepared using the electroless plating method, where Ag NPs were deposited on the surface of BaTiO₃ nanoparticles. The permittivity in the composite BTO@Ag/PVDF was higher than that of BTO/PVDF with the same amount (%) of fillers. The degree of crystallinity, melting temperature, and breakdown strength decreased with increasing filler content. The conductivity of the BTO@Ag/PVDF composite exhibited temperature dependence due to the size of the Ag NPs and the Coulomb blocking effect. It was more noticeable if the filler content of BTO@Ag exceeded 35 vol%.

Carbon-Derived Fillers

Carbon-derived materials are conductive; therefore, they can be used to enhance the dielectric properties of the polymers. For example, Wang et al.⁴⁶ incorporated carbon nanotubes

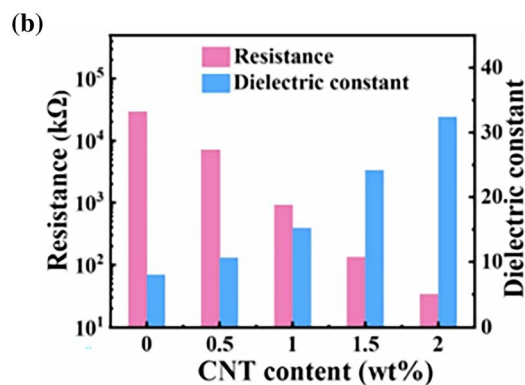
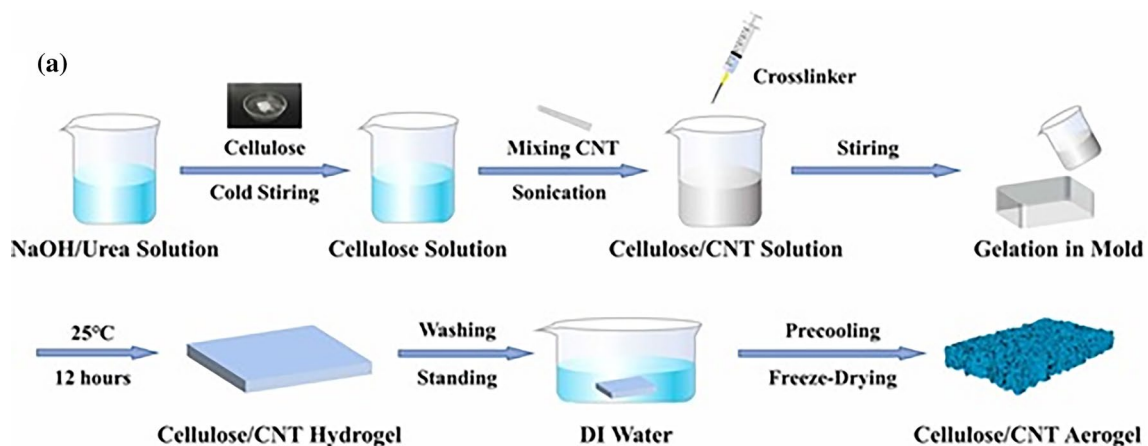


Fig. 5 Dielectric enhanced cellulose-based material for preparation of a triboelectric nanogenerator. (a) Schematic illustration of the fabrication process of cellulose/CNT aerogels. (b) Dielectric constant and

resistance of these cellulose/CNT aerogels at different CNT content. Reprinted with permission from Wang et al.⁴⁶

(CNTs) into a cellulose aerogel to improve the permittivity and the conductivity (Fig. 5). The increase of CNT content led to an increase of permittivity, which was improved from 8 to 15 with 1 wt% CNTs and 32 with 2 wt% CNTs. The cellulose aerogel/CNT composite worked as a triboelectric layer and electrode. The cellulose carbon nanotubes/aerogel TENG (CCA-TENG) exhibited the best performance with 1 wt% CNT. The CCA-TENG exhibited an open-circuit voltage of around 100 V and a short-circuit current of 8 μ A with a 50 N force applied at a frequency of 3 Hz. More than 1 wt% of CNTs in cellulose aerogel led to the decreased electrical output. This was attributed to the effect of agglomeration and the exposure of CNTs in the cellulose aerogel surface.

The insertion of carbon black (CB) nanoparticles into a cement matrix using hydroxyethyl cellulose (HEC) as a dispersant agent produced an excellent dispersion of CB nanoparticles increasing the electric output of the cement/carbon black composite-based TENG.⁴⁷ This increase was induced by the high affinity of the cement with CB nanoparticles due to the abundance of hydroxyl groups. The electrical output of the TENG with cement-CB@HEC composites had an increasing trend with an increasing amount of CB from 0.15 to 0.25 wt%. It was also noted that the cement@HEC TENG (CB = 0 wt%) exhibited a higher output voltage than that of pristine cement-based TENG. The best condition between these TENGs was achieved with the incorporation of 0.225 wt% of HEC and 0.25 wt% of CB. The open-circuit voltage and the short-circuit current were 109 V and 9.1 μ A, respectively. These values were higher than the electrical outputs of the cement-based TENG (32 V and 2.8 μ A) and the cement@HEC TENG (39 V and 3.3 μ V).

The size and concentration of graphite particles (GPs) can also affect the electrical output of a TENG. He et al.⁴⁸ inserted GPs into a PDMS matrix to measure the effect of the particle size. The best performance was achieved with a particle size of 20–40 nm and concentration of 3 wt%. This PDMS@GP-based TENG exhibited an output current of 16.5 μ A and output power density of 3.7 W/m². These values were higher than the non-modified PDMS-based TENG (4.5 μ A and 1.4 W/m²). Smaller NPs (less than 5 nm) caused agglomeration in the PDMS film, while larger NPs (more than 80 nm) did not reach a suitable distribution in the PDMS film. Higher concentrations of NPs (>3 wt%) had a negative impact on the TENG's electrical output performance.

Another conductor that can be used to enhance dielectric properties is graphene, a novel material that is used to fabricate nanocomposites, Harnchana et al.⁴⁹ studied the effect inserting graphene oxide (GO) and sodium dodecyl sulfate (SDS) in poly-(dimethylsiloxane) (PDMS) films. Both solutions, due to the abundance of oxygen functional

groups, caused the accumulation of negative charges in the PDMS film, enhancing its triboelectric properties. The introduction of GO-generated bubbles in the PDMS matrix resulted in a porous structure film and an increase in the specific surface contact area of the film, which was caused by the indissolubility of the GO bubbles. The single-electrode-mode PDMS@GO@SDS TENG achieved the best performance with a concentration of 4 mg/mL of GO, 0.1 M SDS, 5- μ m-thick film, and applied force of 6 N with a frequency of 8 Hz. This TENG exhibited an open-circuit voltage of 412 V and an electrical peak-to-peak current of 45 μ A. These values were higher than those obtained by the non-modified PDMS TENG (125 V and 14 μ A at 5 Hz), PDMS@GO TENG (218 V and 25 μ A at 5 Hz with 4 mg/mL GO), and PDMS@SDS TENG (331 V and 33 μ A at 5 Hz with 0.2 M SDS).

Dai et al.⁵⁰ inserted GO nanosheets into polyvinyl alcohol-polyacrylamide (PVA-PAAm) and double network hydrogel (GPPD hydrogel) to enhance electrical conductivity to 5.51×10^{-3} S/cm. GPPD hydrogel was used as an electrode in the development of a single-electrode-mode TENG. It was able to work under harsh conditions (-80° C), maintaining the same electrical output ($V_{oc} \sim 210$ V at 2 Hz). This anti-freeze ability was attributed to the introduction of ethylene glycol, which formed hydrogen bonds with water. The stability of this TENG also was due to the carbonyl and carboxyl groups on the surface of GO, which increased the density of cross-linking points.

Other Strategies Followed to Enhance Permittivity

The use of inorganic and conductive fillers is the most popular strategy for enhancing the permittivity of polymer dielectrics. However, there are other treatments that can contribute to enhancing permittivity. The polymer matrix can also be reinforced with polymeric fillers. Sun et al.⁵¹ inserted PVA into chitosan (CS) film to enhance TENG performance. Permittivity increased with mixing PVA due to the increase in the interfacial polarization, which occurs at the boundary of crystalline and amorphous regions. With the incorporation of PVA, the crystalline structure increased, and consequently, the boundary between this structure and the amorphous region from CS also increased. The TENG performance based on CS:PVA increased with the PVA amount until reaching a maximum point with a concentration of 5:1. This CS:PVA TENG exhibited a peak-to-peak output voltage of ~ 20 V higher than pure chitosan film (15 V). Concentrations beyond 5:1 showed lower performance. The excessive formation of hydrogen bonds is explained by the bonding of PVA with hydroxyl groups from CS. These bonds limit reorientation space of polarized groups, thus

affecting mobility of polarized groups. After a corona charge injection, the TENG output increased until reaching 100 V.

A combination of fillers and coating has also been used. Vu et al.⁵² synthesized silica nanoparticles and coated the surface of PVDF with an organosilicon compound called 1H,1H,2H,2H-perfluorooctyltriethoxysilane (POTS). It was found that the presence of silica nanoparticles and POTS increased the permittivity of PVDF from 8 to 11.2 at 1 kHz. The TENG fabricated using this modified PVDF showed improved electrical performance, with a voltage output of 6.5 V and a current output of 0.47 μA . In comparison, the TENG fabricated using neat PVDF only achieved a voltage output of 3.1 V and a current output of 0.17 μA .

When a different phase is introduced into a polymeric matrix, interfacial polarization occurs, resulting in an increase in the permittivity of the composite. However, there are other polarization mechanisms that can contribute to the increase in permittivity. Orientational polarization can also affect the permittivity of dielectrics. Cellulose has been used as a triboelectric surface in TENGs because it contains a large number of polar hydroxyl groups ($-\text{OH}$), which initiate orientational polarization mechanisms. Cellulose has a higher permittivity than most linear dielectric polymers. Jangra et al.⁵³ inserted cellulose microfibrils ($\sim 4\text{--}9\ \mu\text{m}$) into a PVDF matrix to enhance its dielectric properties. The permittivity significantly improved at lower frequencies with an increase in cellulose microfibrils. The maximum permittivity obtained was 21 (composite film with 6 wt% of cellulose microfibrils), which is almost three times higher than the permittivity of pure PVDF films ($\epsilon_r = 8$). This cellulose/PVDF composite film was used to fabricate a TENG, which achieved the best output performance when 6 wt% cellulose was incorporated. This TENG exhibited an open-circuit voltage of 61 V, a short-circuit current of 0.382 μA , and a maximum power density of 5.825 $\mu\text{W}/\text{cm}^2$.

Grafting strong polar groups or chain segments onto the surface of cellulose also improves its dielectric properties.⁵⁴ Nie et al.⁵⁵ introduced amine groups into cellulose nanofibril (CNF)-based film through aminosilane modification. This modification involved grafting 3-(2-aminoethylamino)-propyldimethoxymethylsilane (AEAPDMS) onto the surface of CNFs. TENGs prepared using these modified CNFs exhibited an improvement compared to TENGs based solely on pure CNFs. V_{oc} improved from 159 V to 195 V, while I_{sc} increased from 7.0 to 13.4 μA . Liu et al.⁵⁶ evaluated the effect of surface modification on CNF-based films. Different functional groups ($-\text{CF}_2\text{CF}_3$, $-\text{CN}$, $-\text{SH}$, or $-\text{NH}_2$) were introduced onto the CNF-based films by using 3-aminopropyltriethoxysilane (APTES), 3-mercaptopropyltriethoxysilane (MPTES), 3-cyanopropyltriethoxysilane (CPTES), triethoxy-1H,1H,2H,2H-tridecafluoro-n-octylsilane (PFOTES), N-methylaminopropyltrimethoxysilane (NMAPS), and (N,N-dimethylaminopropyl) trimethoxysilane (NNMAPS).

Vertical contact-mode-separation TENGs were fabricated using these CNF-based films. The charge density of these TENGs was compared with that of the unmodified CNF-based TENG. TENGs made with modified CNF-based films showed higher charge densities ($7\text{--}19\ \mu\text{C}/\text{m}^2$) than TENGs made with unmodified CNF-based films ($8.8\ \mu\text{C}/\text{m}^2$). Similar results were also reported for the incorporation of cyanoethyl groups.⁵⁷

Interestingly, the polarization of cellulose can also be modified by controlling the amount of $-\text{OH}$ groups. In fact, the presence of abundant polar $-\text{OH}$ groups in cellulose is a double-edged sword.⁵⁴ The strong polarity and the large number of $-\text{OH}$ groups could improve the permittivity by increasing the number of dipoles. However, at the same time, a large number of $-\text{OH}$ groups can lead to the formation of more hydrogen bonds, which may restrict the movement of $-\text{OH}$ dipoles.^{54,58} Shi et al.⁵⁸ proposed releasing the constrained polar groups of cellulose from the hydrogen bonding network by utilizing epichlorohydrin (ECH). ECH acted as a cross-linker that reacted with $-\text{OH}$ groups, thereby reducing the density of hydrogen bonds and the crystallinity. It allows the movement of polar groups, enhancing permittivity. Regenerated cellulose films cross-linked by ECH (RCCE) were prepared and evaluated, with varying molar ratios between ECH and glucose (GU) units of cellulose. The highest permittivity of 9.7 at $10^3\ \text{Hz}$ was obtained using a molar ratio of ECH to GU of 1:1.

Ion Implantation

Ionic polarization can also modify the permittivity of dielectrics. Sun et al.⁵¹ utilized a corona charge injection method to introduce ions onto the surface of a chitosan:PVA (CS:PVA) composite. In this work, many chloride salts (LiCl , NaCl , CaCl_2 , CuCl_2 , ZnCl_2) were chosen to form metal cations (Li^+ , Na^+ , Ca^{2+} , Cu^{2+} , Zn^{2+} , and Fe^{3+}) onto the surfaces. The best performance was achieved with the addition of 0.01 mol of NaCl in the CS:PVA 5:1 film. It exhibited an output voltage of $\sim 32.5\ \text{V}$, higher than the output voltages of a pure CS-based TENG (17.5 V), CS:PVA 5:1– LiCl (31 V), CS:PVA 5:1– ZnCl_2 (28 V), CS:PVA 5:1– CuCl_2 (22.5 V), CS:PVA 5:1– CaCl_2 (23 V), and CS:PVA 5:1– FeCl_3 (11 V). The introduction of crystal sodium chloride reduced the number of hydrogen bonds, resulting in high electron mobility and enhanced permittivity. The output is higher when the monovalent metal is inserted compared to the divalent and trivalent metal ions. It was attributed to the formation of coordination bonds with a stronger attraction affect. It causes the breakage of hydrogen bonds, but it also restricts the reorientation space of polarized groups, resulting in a decrease in electron mobility and output voltage.

Wang et al.⁵⁹ measured the maximum surface charge density (MSCD) of fluorinated ethylene propylene (FEP) surfaces after ion injection. Commonly, TENGs made without ion injection do not reach the MSCD. The injection of charged ions can provide additional charges in addition to the charge acquired from triboelectrification. Wang's group employed a hand-sized ionized air gun to controllably implant charged ions onto the FEP surface. Negative ions (CO_3^- , NO_3^- , NO_2^- , O_3^- , and O_2^-) were injected onto the surface of FEP due to the material's strong tendency to gain electrons. The negative surface charge does not rely on the chemical properties of the surface. It allows the process to be repeated multiple times until the air reaches the breakdown level. The MSCD was calculated, and it revealed an inverse relationship with the film's thickness. A TENG was fabricated using a negatively charged FEP film with 50 μm of thickness. This TENG exhibited a significant improvement in electrical output compared to a TENG based solely on fluorinated ethylene propylene (FEP). The open-circuit voltage increased from ~ 200 V to ~ 1000 V, and the short-circuit current density increased from 18 to 78 mA/cm^2 under 20 N of applied force. The maximum power output density was ~ 315 W/m^2 , which was achieved using a load resistance of 300 $\text{M}\Omega$.

Fan et al.⁶⁰ utilized ion implantation technology on PTFE and FEP films to increase their polarity, electronegativity, and electron-withdrawing capability. The increase in polar bonds results in a higher permittivity of films, which enhances the performance of the TENG output. The best performance of vertical-contact-mode TENGs fabricated with these films as triboelectric layers was achieved with the implantation dose of 1×10^{14} N ions $/\text{cm}^2$. The PTFE-1E14 film-based TENG exhibited an output voltage of 17.9 V, a surface charge density of 125 $\mu\text{C}/\text{m}^2$, and a current density of 19.2 mA/m^2 . The FEP-1E14 film-based TENG exhibited an output voltage of 27 V, a surface charge density of 230 $\mu\text{C}/\text{m}^2$, and a current density of 24.7 mA/m^2 . Both were higher than TENGs based on pure films: PTFE (3 V, 16 $\mu\text{C}/\text{m}^2$, and 1.65 mA/m^2) and FEP (7 V, 51 $\mu\text{C}/\text{m}^2$, and 8.2 mA/m^2).

Conclusions

Understanding the nature of polymer dielectrics and how to control their permittivity is necessary to select an appropriate approach to enhance the performance of TENGs. The addition of nano and micro fillers in polymer-based dielectrics is a common approach to enhance permittivity by utilizing interfacial polarization. However, the addition of fillers must consider some of the detrimental effects, such as the reduction in the mechanical properties of the resulting material. In addition, when using conductive fillers,

the dielectric properties are drastically increased just below a percolation threshold, so precise control of the amount of filler used is advised. Beyond the percolation threshold, the composite will behave as a conductive material, and triboelectric generation will not be possible. An appropriate selection of the strategy to control the permittivity of the dielectrics used in the fabrication of TENGs is crucial for achieving high output performance.

Acknowledgments This research was funded by CONCYTEC PROCIENCIA, under the grant "Applied and technology development research projects 2020-02" (grant no. 166-2020-FONDECYT). The authors would like to thank the Vice-Rectorate for Research of the Pontificia Universidad Catolica del Peru (VRI-PUCP) for financial support (grant PI0866).

Funding This study was funded by CONCYTEC PROCIENCIA and the Pontificia Universidad Catolica del Peru (VRI-PUCP).

Conflict of interest The authors have no relevant financial or non-financial interests to disclose.

References

1. F.G. Torres, and G.E. De-la-Torre, Polysaccharide-based triboelectric nanogenerators: a review. *Carbohydr. Polym.* 251, 117055 (2021). <https://doi.org/10.1016/j.carbpol.2020.117055>.
2. F.-R. Fan, Z.-Q. Tian, and Z. Lin Wang, Flexible triboelectric generator. *Nano Energy* 1, 328–334 (2012). <https://doi.org/10.1016/j.nanoen.2012.01.004>.
3. S. Niu, and Z.L. Wang, Theoretical systems of triboelectric nanogenerators. *Nano Energy* 14, 161–192 (2015). <https://doi.org/10.1016/j.nanoen.2014.11.034>.
4. S. Niu, S. Wang, L. Lin et al., Theoretical study of contact-mode triboelectric nanogenerators as an effective power source. *Energy Environ. Sci.* 6, 3576 (2013). <https://doi.org/10.1039/c3ee42571a>.
5. L.-H. Lee, Dual mechanism for metal-polymer contact electrification. *J. Electrostat.* 32, 1–29 (1994). [https://doi.org/10.1016/0304-3886\(94\)90026-4](https://doi.org/10.1016/0304-3886(94)90026-4).
6. F. Saurenbach, D. Wollmann, B.D. Terris, and A.F. Diaz, Force microscopy of ion-containing polymer surfaces: morphology and charge structure. *Langmuir* 8, 1199–1203 (1992). <https://doi.org/10.1021/la00040a030>.
7. J.-W. Zha, M.-S. Zheng, B.-H. Fan, and Z.-M. Dang, Polymer-based dielectrics with high permittivity for electric energy storage: a review. *Nano Energy* 89, 106438 (2021). <https://doi.org/10.1016/j.nanoen.2021.106438>.
8. Z. Yang, D. Yue, Y. Yao et al., Energy storage application of all-organic polymer dielectrics: a review. *Polymers (Basel)* 14, 1160 (2022). <https://doi.org/10.3390/polym14061160>.
9. Ahmad Z (2012) Polymer Dielectric Materials. In: Dielectric Material. InTech
10. V. Bobnar, B. Vodopivec, A. Levstik et al., Dielectric properties of relaxor-like vinylidene fluoride–trifluoroethylene-based electroactive polymers. *Macromolecules* 36, 4436–4442 (2003). <https://doi.org/10.1021/ma034149h>.
11. A.R. Blythe, and D. Bloor, *Electrical Properties of Polymers*, 2nd ed., (Cambridge: Cambridge University Press, 2005).
12. K.-C. Kao, *Dielectric Phenomena in Solids: with Emphasis on Physical Concepts of Electronic Processes* (Boston: Elsevier Academic Press, 2004).

13. T.V.K. Prateek, and R.K. Gupta, Recent progress on ferroelectric polymer-based nanocomposites for high energy density capacitors: synthesis, dielectric properties, and future aspects. *Chem. Rev.* 116, 4260–4317 (2016). <https://doi.org/10.1021/acs.chemrev.5b00495>.
14. R. Popielarz, C.K. Chiang, R. Nozaki, and J. Obrzut, Dielectric properties of polymer/ferroelectric ceramic composites from 100 Hz to 10 GHz. *Macromolecules* 34, 5910–5915 (2001). <https://doi.org/10.1021/ma001576b>.
15. S. Siddabattuni, T.P. Schuman, and F. Dogan, Dielectric properties of polymer-particle nanocomposites influenced by electronic nature of filler surfaces. *ACS Appl. Mater. Interfaces* 5, 1917–1927 (2013). <https://doi.org/10.1021/am3030239>.
16. H.K. Kim, and F.G. Shi, Thickness dependent dielectric strength of a low-permittivity dielectric film. *IEEE Trans. Dielectr. Electr. Insul.* 8, 248–252 (2001). <https://doi.org/10.1109/94.919946>.
17. Z. Dang, J. Yuan, S. Yao, and R. Liao, Flexible nanodielectric materials with high permittivity for power energy storage. *Adv. Mater.* 25, 6334–6365 (2013). <https://doi.org/10.1002/adma.201301752>.
18. Z.-M. Dang, J.-K. Yuan, J.-W. Zha et al., Fundamentals, processes and applications of high-permittivity polymer–matrix composites. *Prog. Mater. Sci.* 57, 660–723 (2012). <https://doi.org/10.1016/j.pmatsci.2011.08.001>.
19. Z.-M. Dang, Y.-H. Lin, and C.-W. Nan, Novel ferroelectric polymer composites with high dielectric constants. *Adv. Mater.* 15, 1625–1629 (2003). <https://doi.org/10.1002/adma.200304911>.
20. Z.-M. Dang, Y. Shen, and C.-W. Nan, Dielectric behavior of three-phase percolative Ni–BaTiO₃/polyvinylidene fluoride composites. *Appl. Phys. Lett.* 81, 4814–4816 (2002). <https://doi.org/10.1063/1.1529085>.
21. D. Yang, H. Xu, and W. Yu, Comparative study on the dielectric properties of three polyvinylidene fluoride nanocomposites incorporated with carbon filler. *J. Thermoplast. Compos. Mater.* 31, 1102–1111 (2018). <https://doi.org/10.1177/0892705717734601>.
22. C.-W. Nan, Physics of inhomogeneous inorganic materials. *Prog. Mater. Sci.* 37, 1–116 (1993). [https://doi.org/10.1016/0079-6425\(93\)90004-5](https://doi.org/10.1016/0079-6425(93)90004-5).
23. W. Seung, H.J. Yoon, T.Y. Kim et al., Boosting power-generating performance of triboelectric nanogenerators via artificial control of ferroelectric polarization and dielectric properties. *Adv. Energy Mater.* 7, 52 (2017). <https://doi.org/10.1002/AENM.201600988>.
24. J. Chen, H. Guo, X. He et al., Enhancing performance of triboelectric nanogenerator by filling high dielectric nanoparticles into sponge PDMS film. *ACS Appl. Mater. Interfaces* 8, 736–744 (2016). <https://doi.org/10.1021/ACSAMI.5B09907>.
25. Z. Zheng, J. Xia, B. Wang, and Y. Guo, Hierarchically designed nanocomposites for triboelectric nanogenerator toward biomechanical energy harvester and smart home system. *Nano Energy* 95, 107047 (2022). <https://doi.org/10.1016/j.nanoen.2022.107047>.
26. Y. Shao, C.P. Feng, B.W. Deng et al., Facile method to enhance output performance of bacterial cellulose nanofiber based triboelectric nanogenerator by controlling micro-nano structure and dielectric constant. *Nano Energy* 62, 620–627 (2019). <https://doi.org/10.1016/j.nanoen.2019.05.078>.
27. D. Tantraviwat, M. Ngamyngouid, W. Sripumkhai et al., Tuning the dielectric constant and surface engineering of a BaTiO₃ / porous PDMS composite film for enhanced triboelectric nanogenerator output performance. *ACS Omega* 6, 29765–29773 (2021). <https://doi.org/10.1021/acsomega.1c04222>.
28. X. Du, Y. Liu, J. Wang et al., Improved triboelectric nanogenerator output performance through polymer nanocomposites filled with core–shell-structured particles. *ACS Appl. Mater. Interfaces* 10, 25683–25688 (2018). <https://doi.org/10.1021/acsami.8b05966>.
29. L. Xie, X. Huang, Y. Huang et al., Core@Double-shell structured BaTiO₃-polymer nanocomposites with high dielectric constant and low dielectric loss for energy Storage Application. *J. Phys. Chem. C* 117, 22525–22537 (2013). <https://doi.org/10.1021/JP407340N>.
30. V.A. Cao, S. Lee, M. Kim et al., Output power density enhancement of triboelectric nanogenerators via ferroelectric polymer composite interfacial layers. *Nano Energy* 67, 104300 (2020). <https://doi.org/10.1016/j.nanoen.2019.104300>.
31. L. Dong, C. Xiong, H. Quan, and G. Zhao, Polyvinyl-butyril/lead zirconate titanates composites with high dielectric constant and low dielectric loss. *Scr. Mater.* 55, 835–837 (2006). <https://doi.org/10.1016/j.scriptamat.2006.07.001>.
32. W. Wang, J. Zhang, Y. Zhang et al., Remarkably enhanced hybrid piezo/triboelectric nanogenerator via rational modulation of piezoelectric and dielectric properties for self-powered electronics. *Appl. Phys. Lett.* 116, 524 (2020). <https://doi.org/10.1063/1.5134100>.
33. M. Kim, D. Park, Md.M. Alam et al., Remarkable output power density enhancement of triboelectric nanogenerators via polarized ferroelectric polymers and bulk MoS₂ composites. *ACS Nano* 13, 4640–4646 (2019). <https://doi.org/10.1021/acsnano.9b00750>.
34. W. Bunriw, V. Harnchana, C. Chanthad, and V.N. Huynh, Natural rubber-TiO₂ nanocomposite film for triboelectric nanogenerator application. *Polymers (Basel)* 13, 2213 (2021). <https://doi.org/10.3390/polym13132213>.
35. Z. Fang, K.H. Chan, X. Lu et al., Surface texturing and dielectric property tuning toward boosting of triboelectric nanogenerator performance. *J. Mater. Chem. A Mater.* 6, 52–57 (2018). <https://doi.org/10.1039/C7TA07696G>.
36. Q.G. Chi, L. Gao, X. Wang et al., Effects of magnetic field treatment on dielectric properties of CCTO@Ni/PVDF composite with low concentration of ceramic fillers. *AIP Adv.* 5, 52 (2015). <https://doi.org/10.1063/1.4935270>.
37. L.K. Anlin, K.V. Vijoy, K. Pradeesh et al., Effects of metal nanoparticles on the performance of PDMS based triboelectric nanogenerators. *Physica B Condens. Matter.* 639, 413952 (2022). <https://doi.org/10.1016/J.PHYSB.2022.413952>.
38. M.N. Biutty, J.M. Koo, M. Zakia et al., Dielectric control of porous polydimethylsiloxane elastomers with Au nanoparticles for enhancing the output performance of triboelectric nanogenerators. *RSC Adv.* 10, 21309–21317 (2020). <https://doi.org/10.1039/D0RA03522J>.
39. J. Chun, J.W. Kim, W.S. Jung et al., Mesoporous pores impregnated with Au nanoparticles as effective dielectrics for enhancing triboelectric nanogenerator performance in harsh environments. *Energy Environ. Sci.* 8, 3006–3012 (2015). <https://doi.org/10.1039/C5EE01705J>.
40. I. Appamato, W. Bunriw, V. Harnchana et al., Engineering triboelectric charge in natural rubber–Ag nanocomposite for enhancing electrical output of a triboelectric nanogenerator. *ACS Appl. Mater. Interfaces* 15, 973–983 (2023). <https://doi.org/10.1021/acsami.2c17057>.
41. Y. Zhang, Y. Shao, C. Luo et al., Preparation of a high-performance chitosan-based triboelectric nanogenerator by regulating the surface microstructure and dielectric constant. *J. Mater. Chem. C Mater.* 11, 260–268 (2023). <https://doi.org/10.1039/D2TC04262B>.
42. X. Chen, X. Pu, T. Jiang et al., Tunable optical modulator by coupling a triboelectric nanogenerator and a dielectric elastomer. *Adv. Funct. Mater.* 27, 69 (2017). <https://doi.org/10.1002/ADFM.201603788>.
43. K. Shi, H. Zou, B. Sun et al., Dielectric modulated cellulose paper/PDMS-based triboelectric nanogenerators for wireless transmission and electropolymerization applications. *Adv. Funct. Mater.* 30, 36 (2020). <https://doi.org/10.1002/ADFM.201904536>.

44. L. Ren, X. Meng, J.W. Zha, and Z.M. Dang, Coulomb block effect inducing distinctive dielectric properties in electroless plated barium titanate@silver/poly(vinylidene fluoride) nanocomposites. *RSC Adv.* 5, 65167–65174 (2015). <https://doi.org/10.1039/C5RA11496A>.
45. H. Oh, S.S. Kwak, B. Kim et al., Highly conductive ferroelectric cellulose composite papers for efficient triboelectric nanogenerators. *Adv. Funct. Mater.* 29, 1–6 (2019). <https://doi.org/10.1002/adfm.201904066>.
46. Z. Wang, C. Chen, L. Fang et al., Biodegradable, conductive, moisture-proof, and dielectric enhanced cellulose-based triboelectric nanogenerator for self-powered human-machine interface sensing. *Nano Energy* 107, 63 (2023). <https://doi.org/10.1016/j.nanoen.2022.108151>.
47. S. Kuntharin, V. Harnchana, A. Klamchuen et al., Boosting the power output of a cement-based triboelectric nanogenerator by enhancing dielectric polarization with highly dispersed carbon black nanoparticles toward large-scale energy harvesting from human footsteps. *ACS Sustain. Chem. Eng.* 10, 4588–4598 (2022). <https://doi.org/10.1021/acssuschemeng.1c08629>.
48. X. He, H. Guo, X. Yue et al., Improving energy conversion efficiency for triboelectric nanogenerator with capacitor structure by maximizing surface charge density. *Nanoscale* 7, 1896–1903 (2015). <https://doi.org/10.1039/C4NR05512H>.
49. V. Harnchana, N.H. Van, W. He et al., Enhanced power output of a triboelectric nanogenerator using poly(dimethylsiloxane) modified with graphene oxide and sodium dodecyl sulfate. *ACS Appl. Mater. Interfaces* 10, 25263–25272 (2018). <https://doi.org/10.1021/acsami.8b02495>.
50. X. Dai, Y. Long, B. Jiang et al., Ultra-antifreeze, ultra-stretchable, transparent, and conductive hydrogel for multi-functional flexible electronics as strain sensor and triboelectric nanogenerator. *Science* 15, 5461–5468 (2022).
51. J. Sun, H. Choi, S. Cha et al., Highly enhanced triboelectric performance from increased dielectric constant induced by ionic and interfacial polarization for chitosan based multi-modal sensing system. *Adv. Funct. Mater.* 32, 245 (2022). <https://doi.org/10.1002/ADFM.202109139>.
52. D.L. Vu, C.D. Le, and K.K. Ahn, Polyvinylidene fluoride surface polarization enhancement for liquid-solid triboelectric nanogenerator and its application. *Polymers (Basel)* 14, 960 (2022). <https://doi.org/10.3390/polym14050960>.
53. M. Jangra, A. Thakur, S. Dam, and S. Hussain, Enhanced dielectric properties of freestanding, flexible, hydrophobic cellulose/poly(vinylidene fluoride) composite films. *J. Polym. Sci.* 61, 334–345 (2023). <https://doi.org/10.1002/pol.20220512>.
54. Q. Luo, H. Shen, G. Zhou, and X. Xu, A mini-review on the dielectric properties of cellulose and nanocellulose-based materials as electronic components. *Carbohydr. Polym.* 303, 2489 (2023). <https://doi.org/10.1016/j.carbpol.2022.120449>.
55. S. Nie, C. Cai, X. Lin et al., Chemically functionalized cellulose nanofibrils for improving triboelectric charge density of a triboelectric nanogenerator. *ACS Sustain. Chem. Eng.* 8, 18678–18685 (2020). <https://doi.org/10.1021/acssuschemeng.0c07531>.
56. Y. Liu, Q. Fu, J. Mo et al., Chemically tailored molecular surface modification of cellulose nanofibrils for manipulating the charge density of triboelectric nanogenerators. *Nano Energy* 89, 56 (2021). <https://doi.org/10.1016/j.nanoen.2021.106369>.
57. N. Wang, W. Zhang, Z. Li et al., Dual-electric-polarity augmented cyanoethyl cellulose-based triboelectric nanogenerator with ultrahigh triboelectric charge density and enhanced electrical output property at high humidity. *Nano Energy* 103, 107748 (2022). <https://doi.org/10.1016/j.nanoen.2022.107748>.
58. S.C. Shi, C. Chen, J.L. Zhu et al., Environmentally friendly regenerated cellulose films with improved dielectric properties via manipulating the hydrogen bonding network. *Appl. Phys. Lett.* 119, 69 (2021). <https://doi.org/10.1063/5.0056164/40820>.
59. S. Wang, Y. Xie, S. Niu et al., Maximum surface charge density for triboelectric nanogenerators achieved by ionized-air injection: methodology and theoretical understanding. *Adv. Mater.* 26, 6720–6728 (2014). <https://doi.org/10.1002/ADMA.201402491>.
60. Y. Fan, S. Li, X. Tao et al., Negative triboelectric polymers with ultrahigh charge density induced by ion implantation. *Nano Energy* 90, 106574 (2021). <https://doi.org/10.1016/j.nanoen.2021.106574>.

Publisher's Note Springer Nature remains neutral with regard to jurisdictional claims in published maps and institutional affiliations.

Springer Nature or its licensor (e.g. a society or other partner) holds exclusive rights to this article under a publishing agreement with the author(s) or other rightsholder(s); author self-archiving of the accepted manuscript version of this article is solely governed by the terms of such publishing agreement and applicable law.